Three-dimensional hierarchical mesoporous carbon for regenerative electrochemical dopamine sensor

Shuyuan Wang [a,b], Peng Guo [a], Guanshui Ma [a], Jing Wei [a,b], Zhenyu Wang [a], Li Cui [a], Lili Sun [a], Aiying Wang [a,b,c,*]

[a] Key Laboratory of Marine Materials and Related Technologies, Zhejiang Key Laboratory of Marine Materials and Protective Technologies, Ningbo Institute of Materials Technology and Engineering, Chinese Academy of Sciences, Ningbo 315201, China
[b] Center of Materials Science and Optoelectronics Engineering, University of Chinese Academy of Sciences, Beijing 100049, China
[c] Ningbo Institute of Industrial Technology, Chinese Academy of Sciences, Ningbo 315201, China

ARTICLE INFO

ABSTRACT

The detection of dopamine (DA) based on electrochemical sensor is of great importance to human diseases diagnosis and treatment. However, such sensors usually faced with the performance deterioration due to serious dopamine fouling. Herein, we fabricated a three-dimensional (3D) porous carbon sheet with hierarchical ordered mesopores by a facile dual-template method, the integrated electrochemical sensor was further discussed in terms of the evolution of porous structure. Results showed that the hierarchical porous structure would provide more mass transport channels and larger active area, resulting in higher sensitivity. In particular, the 3D framework could withstand strong ultrasound cleaning and maintained the superior electrochemical properties with high repeatability after the ultrasonic cleaning for dopamine fouling. The integrated sensor based on 3D porous carbon with high sp^2 content presented the excellent performance toward DA detection with wide linear range from 800 nM to 400 μM, low detection limit of 100 nM as well as good selectivity to routine interference substances. It can be said that the constructed 3D hierarchical mesoporous carbon provides the great potential to be a promising material for DA electrochemical sensing platform construction.

© 2020 Elsevier Ltd. All rights reserved.

1. Introduction

Dopamine(DA), a catecholamine neurotransmitter, which makes great sense to cardiovascular, renal, hormonal functions and human central nervous system [1]. Abnormal of dopamine level is related to the development of many diseases, such as Parkinson's disease, Alzheimer's disease, schizophrenia, hypertension and heart failure [2,3]. Therefore, the accurate determination of DA is significant to diagnosis, treatment and prevention of diseases [4,5]. So far, several analytical methods for DA have been developed, including gas chromatography-mass spectrometry [6], chemiluminescence [7], colorimetry [8], electrochemical analysis [9,10], spectrophotometry [11], electrophoresis [12], electrochemical and high-performance liquid chromatography [13]. These detection technologies have their own advantages and are suitable for different application scenarios. In particular, the electrochemical analysis has attracted a lot of attention in DA sensing field, due to easy handling, fast response, inexpensive tools and high sensitivity [14,15].

In electrochemical analysis, the performance of sensors often depends on its electrode material. Owning to the special properties of wide potential window, chemical inertness, good conductivity and biocompatibility [16,17], carbon nano-materials have been widely used in the construction of DA electrochemical sensors [18], such as graphene [19–21], graphene oxide [22], carbon nanotubes (CNT) [23], C_{60} [24], hollow carbon sphere [25] and porous carbon [26,27]. Particularly, porous carbon is an attractive branch of carbon nano-materials with appealing characteristics including three dimension (3D) structure, stable framework, tunable pore size, large specific area, abundant sources, low toxicity and chemical stability [28,29]. Hierarchical porous carbon combined pores of diverse sizes, among which macropores enhanced the diffusion, mesopores promoted mass transfer and micropores increased specific area [30], improving DA sensing performance synergistically. Dong et al. prepared hierarchical porous carbon with mesopores and macropores through pyrolysis of sodium citrate and further the porous carbon powders were modified on glassy carbon

electrode (GCE), which showed more active sites, faster electron transfer rate, and better electro-catalytical properties to DA detection than conventional GCE [31]. Likewise, Liu et al. fabricated a GCE sensor modified by ordered mesoporous carbon which was prepared by hard-template method, and the sensor showed excellent sensitivity and selectivity for electrochemical sensing of DA [32]. Hence, hierarchical porous carbons were proved to be a potential material for constructing highly sensitive electrochemical platform of DA.

However, fouling usually pose a threat to the DA electrochemical analysis [33]. Since DA molecular is easy to oxidize, it would polymerize and form insulating film adhering on the electrode surface, which often cause diminishing in electrode response [34,35]. Palomaki et al. researched the DA fouling effect and observed polydopamine granules on electrode surfaces, which decreased the electrode active area and led to the passivation of the electrodes, especially at neutral and alkaline pH [36,37]. In order to eliminate the stubborn DA pollutants and regenerate the electrode after detection process, ultrasonic cleaning was considered strongly as an alternative strategy [38]. Normally, a porous carbon electrochemical sensor was fabricated by drop-casting method in which porous carbon was made into powder and distributed on the surface of commercial electrodes (such as GCE) and then dried [17,28,32,39–42]. However, this kind of porous carbon modified electrode could not be effectively cleaned, because the porous carbon and electrode substrate were combined by Van der Waals forces, which performed as a kind of weak interface bonding [38]. Although addition of Nafion could improve the interfacial combination to some extent [43], it also caused the problem of lower conductivity. Therefore, the overall 3D porous carbon was expected to overcome this problem through ultrasonic cleaning owning to its stable framework. And it is attractive to fabricate a DA electrochemical sensing platform, which could avoid the interface problem and meanwhile own the advantages of 3D hierarchical porous carbon structure.

In this work, an overall 3D hierarchical porous carbon electrode was fabricated, which could withstand ultrasonic cleaning, for electrochemical analysis of DA detection. Hierarchical macropores and ordered mesopores have been constructed through dual-template method with polyethylene terephthalate (PET) fibric as hard template and triblock polymer F127 as soft template, respectively. Instead of using drop-casting method, this sensor was directly fabricated by an overall porous carbon sheet so that the weak combination could be avoided. The sensing performance and supersonic stability of this electrode were evaluated in terms of the evolution of hierarchical porous structure.

2. Experiment

2.1. Reagents and materials

PET non-woven fabrics were purchased from Dongguan Jialianda Non-woven Cloth Co. Ltd., China. Reagents in this experiment were all analytical grade and all the solutions were prepared in deionized water. Phenol, formaldehyde solution (37 wt% in H_2O), Tetrahydrofuran (THF), Pluronic® F-127, P-toluenesulfonic acid and NaOH were obtained from Sigma–Aldrich. $K_3[Fe(CN)_6]$ was purchased from RHAWN. Hexaammineruthenium (III) chloride was bought from Energy Chemical. Chloroform ($CHCl_3$), Uric acid (UA), KH_2PO_4, NaCl, $MgSO_4$, KCl and Glucose were purchased from Sinopharm Chemical Reagent Co. Ltd., China. Na_2HPO_4 and Dopamine hydrochloride were obtained from Aladdin Reagent (Shanghai) Co., Ltd., China. Phosphate buffer solution (PBS) at pH=7.0 were mixed by 0.1 M KH_2PO_4, 0.1 M Na_2HPO_4 and 0.1 M NaCl.

2.2. Sample preparation

The phenol-formaldehyde resol was prepared by formaldehyde solution and phenol in the presence of NaOH as catalyst according to previous publication [44]. After 3.06 g phenol was added and melted in a three-mouth flask at 45 °C, 0.65 g NaOH solution (30 wt%) was dropped into phenol and stirred for 10 mins. Then 5.25 g of formaldehyde solution (37 wt% in H_2O) was gradually instilled in the solution and reaction went on for 2 h at 75 °C in nitrogen atmosphere. After the solution cooling down to room temperature, 0.62 g P-toluenesulfonic acid was added to adjust the solution pH to 7. Next, a rotation evaporation process was carried on to remove water from the as prepared precursor. Then the precursor was dissolved in the mixture of THF and $CHCl_3$ (THF: $CHCl_3$=1:1 wt), in which NaOH was removed by suction filtration through a PTFE filter (0.4 μm). After another rotation evaporation step, the precursor was dissolved in ethanol with a concentration of 20 wt%, and the resol solution was successfully prepared.

The hierarchical porous carbon was prepared as follow. Frist, PET non-woven fabrics were washed by deionized water and dried in oven, then they were immersed for 12 h in the solution mixed by 5.0 g phenol-formaldehyde resol solution (20 wt% in ethanol) and 11.5 g F127 solution (F127 dissolved in10.0 g ethanol). After that, an evaporation self-assembly process was performed with the container lid opened, followed by polymerization heat treatment at 120 °C for 12 h. Pyrolysis process was conducted in argon atmosphere of 100 sccm flow rate with a programmed heat treatment, in which the temperature was first increased from room temperature to 350 °C for 3 h, then increased to 600 °C for 1 min and 900 °C for 1 hour.

The working electrode for dopamine detection was fabricated as follow. First, the porous carbon sheet was cut into 1.2 cm × 1.2 cm pieces and connected by copper wire pasted by Ag paint with a PET sheet as substrate. Then, the edges and joints were covered by silicone resin with an active window of 1 cm × 1 cm area left.

2.3. Characterization

The morphology of material were characterized by scanning electron microscopy (SEM) (Verios G4 UC, Thermo scientific, USA and QUANTA 250 FEG, FEI, USA) and a transmission electron microscope (TEM) (Tecnai F20, FEI, USA). Porous carbon sample was characterized by Raman spectra (InVia Reflex, Renishaw, UK) with a 532 nm exciting wavelength. The surface chemical properties were investigated by fourier transform infrared spectroscopy (FTIR) (Nicolet 6700, Thermo, USA). Small-angle X-ray scattering (SAXS) pattern was collected on X-ray powder diffractometer (D8 ADVANCE DAVINCI, Bruker, Germany) using a Cu K_α X-ray source (λ = 0.154 nm) at 40 kV and 40 mA. N_2 adsorption-desorption isotherms were carried out by a gas adsorption analyzer (Autosorb iQ, Quantachrome, USA) at 77.35 K. The pore size distribution was calculated from the adsorption isotherms with Barrett–Joyner–Halenda (BJH) method. Electrochemical measurements were conducted with an electrochemical workstation (CHI840D, CH Instruments, China) in a conventional three-electrode electrochemical cell system, which consisted of an Ag/AgCl (KCl saturated) as reference electrode, a platinum plate as auxiliary electrode and the porous carbon electrodes as working electrodes, respectively. Before test, the porous carbon electrodes were thoroughly rinsed in deionized water and then dried in the oven at 30 °C. The solutions were bubbled with argon gas for at least 15 mins to deoxygenate before test and blanked with argon flow during test to avoid DA self-polymerization. All the experiments were carried out at room temperature (25 °C).
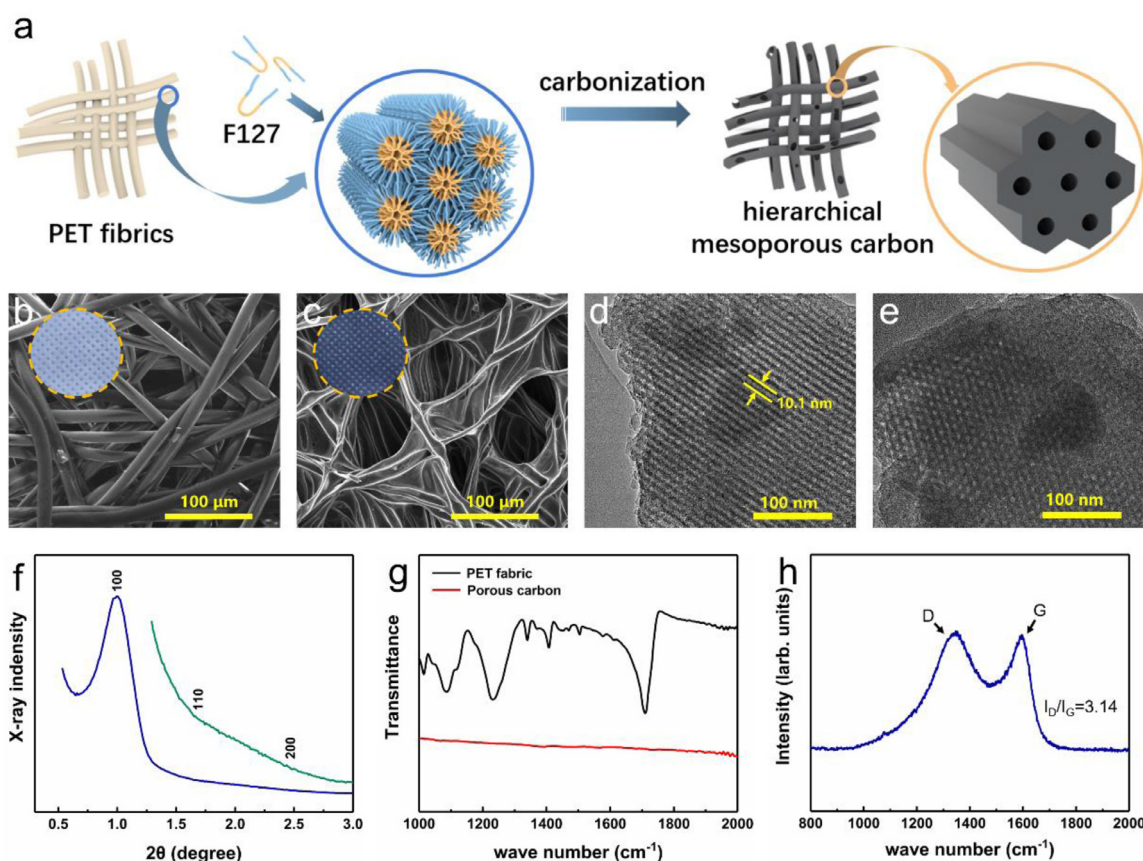
Fig. 1. Scheme of mesoporous carbon formation (a); SEM image of pristine PET fibric (b) and mesoporous carbon (c), insert is the corresponding optical photo; TEM image of mesoporous carbon viewed from [110] (d) and [100] (e) direction. SAXS pattern of mesoporous carbon (f); FT-IR spectrum of pristine PET and mesoporous carbon (g); Raman shift of mesoporous carbon (h).

3. Result and discussion

3.1. Characteristics of 3D structured hierarchical porous carbon

Fig. 1a illustrated the fabrication progress and the formation mechanism of the 3D porous carbon in this work. First, phenolic resin film and F127 hollow micelle adhered to PET fabrics, which was driven by evaporation-induced self-assembly due to the amphiphilic properties of triblock polymers F127. Then, the 3D carbon skeleton with abundant hollow cylindrical macropores and ordered mesopores were formed after a carbonization process, where the PET fibers and F127 were easy to decompose while phenolic resin were thermosetting. The morphology of pristine PET fibric and the as prepared porous carbon were studied by SEM and TEM analysis with typical result shown in Fig. 1b-e. The pristine PET non-woven fibric was a flat sheet (insert of Fig. 1b) which consist of crosslinking PET fibers with abundant macropores (Fig. 1b). From the insert of Fig. 1c, we can see the as prepared porous carbon maintained the shape of PET fabrics. As was shown in Fig. 1c, an overall porous carbon network made up of cross-linked fibers was observed, in which messes of cylindrical macropores with the diameter from 10 μm to 15 μm were formed because of PET fibers decomposition. Further, detailed structure was observed in TEM image. As was shown in Fig. 1d and Fig. 1e, large domains of highly ordered stripe-like arrays along [110] direction and the ordered hexagonally arranged pores along [100] direction were visible, indicating a well-developed typical 2D hexagonal mesoporous structure. According to the TEM image, the pore size and the hole pitch were estimated to be 3–5 nm and 10.1 nm, respectively. The small-angle X-ray scattering (SAXS) also confirmed the mesoporous structure.

In Fig. 1f, an intense diffraction peak and two very weak peaks appeared with 2θ range from 0.5° to 3°, which was attribute to [100], [110], [200] reflection, respectively, indicating the well regularity of hexagonal space group (p6mm) [45,46]. The Interplanar crystal spacing d_{100} value could be calculated by Bragg equation $d_{100} = \lambda/2\sin\theta$ and the unit cell parameter a_0 was calculated by $a_0 = 2d_{100}/\sqrt{3}$ [47]. According to calculation, the unit cell parameter a_0 was 10.1 nm, which was in good agreement with TEM results.

The chemical composition of porous carbon was also investigated by FT-IR and Raman spectrum. FT-IR showed the evolution of functional group from PET fabrics to porous carbon. In Fig. 1g, several characteristic peaks were observed on the PET spectrum: the peak at 1247 cm^{-1} caused by the vibration of the ester group, the peak of 1470 ~ 1350 cm^{-1} originated from the ethylene glycol fragment and the peak at 1717 cm^{-1} due to the stretching vibration of the ester carbonyl group [44]. While on the spectrum of porous carbon, those corresponding peaks disappeared, since these oxygen-containing groups were easily to break and decompose during pyrolysis. Raman spectrum of porous carbon was shown in Fig. 1h, in which there were two typical peaks at 1346.6 cm^{-1} and 1595.3 cm^{-1} corresponding to the D and G band, indicating a typical structure of amorphous carbon [48]. The high I_D/I_G of 3.14 indicated the high content of plane and lattice edges as well as well as high sp^2 cluster content, which could increase the surface reactivity and electron transport of porous carbon [49].

To further study the pore size and distribution of porous carbon, nitrogen absorption-desorption isotherms were analyzed at 77.35 K. As shown in Fig. 2a, the isotherm shape of F127 added porous carbon was close to type-IV curve [50] which showed
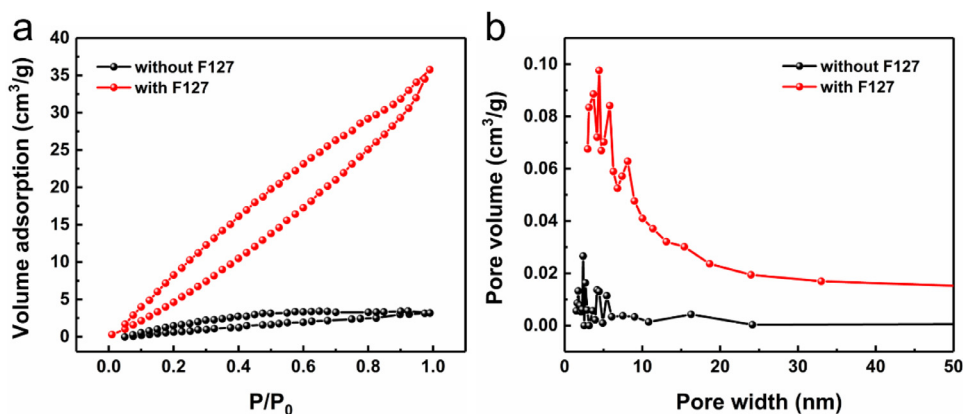
Fig. 2. N$_2$ adsorption/desorption isotherms (a) and the pore size distributions (b) of F127 added and no F127 added porous carbon.

much higher nitrogen adsorption capacity than the one without F127 added. The surface area increased from 18.14 m^{2}g^{-1} to 58.25 m^{2}g^{-1} with the addition of F127, which was calculated by Brunner−Emmet−Teller (BET) model [51]. Furthermore, the pore size distributions were calculated from absorption branch using the BJH model as was shown in Fig. 2b. Compared to the porous carbon without F127 added, the F127 added one showed a large number of uniform mesopores at 4.4 nm, suggesting the well-developed mesopores. Therefore, a large number of mesopores was constructed with the addition of triblock copolymers F127. In order to address the role of high surface area, the electrochemical active area of porous carbon electrode and GCE were calculated by CV curves in 10 mM K$_3$[Fe(CN)$_6$] solution according to the Randles-Sevick equation [52]: $ip = 268,600 \, n^{\frac{3}{2}} A D^{\frac{1}{2}} C v^{\frac{1}{2}}$. In Fig. S2, porous carbon electrode showed much higher current signal than GCE. Correspondingly, the electrochemical active area of porous carbon electrode (1.295 cm^2) obviously exceeded that of GCE (0.189 cm^2), implying that the high active area would be one of the reasons for signal enhancement.

3.2. Ultrasonic stability of porous carbon electrode

The ultrasonic resistance of the porous carbon electrode was evaluated. The electrochemical performance and structure changes of this porous carbon electrode were compared before and after a designed long-term ultrasonic cleaning simulation. The electrochemical performance was measured by cyclic voltammetry (CV) curves, which was performed with the addition of 10 mM potassium ferricyanide (K$_3$[Fe(CN)$_6$]) in 1 M HCl solution with the scan rate ranging from 20 mV/s to 200 mV/s. At the beginning, a new porous carbon electrode was tested shown in Fig. 3a and Fig. 3b. The oxidation and reduction peak current density were all increased with scan rate shown in Fig. 3a. Furthermore, the peak current density showed a linear relationship with the square root of scan rates (shown in Fig. 3b), which indicated that the chemical reaction was controlled by diffusion process [53]. Then, an ultrasonic bath was conducted in deionized water to test the long-term resistance of porous carbon electrode for 10 min, 30 min, 60 min, 120 min and 200 min at the power of 200 w. As shown in Fig. 3c, slightly changes were observed in the CV curves after different ultrasonic time, which were nearly negligible with only 1.37% difference of peak density shown in the magnified view of oxidation peak current position (Fig. 3d). Even after 200 min ultrasonic bath, the CV curves still maintained high degree of similarity in graphical shape compared to that of origin electrode (see Fig. 3e). Fig. 3f revealed the linear growth of peak current density with the square root of scan rates, which showed good stability after 200 min ultrasonic cleaning. To further investigate the

ultrasonic stability of porous carbon, the micro structure was characterized by SEM and TEM. From the scanning electron microscope image shown in Fig. S1a, a porous structure formed by cross-linked carbonized fibers was obtained, in which the fibers still remained intact and showed almost no difference from the porous structure before ultrasonic. At the nanoscale, the mesopores were found to keep the same morphology as the pristine porous structure in TEM image shown in Fig.S1b. The above pictures proposed that the porous structure was stable enough to withstand 200 min ultrasound and the surface structure kept stable, which played a significant role in electrode reaction. Therefore, the as prepared porous carbon material has the potential to become an effective electrode material in electrochemical sensing platform for biofouling regents such as dopamine.

The resistance to DA contamination of porous carbon electrode was investigated by CV method and FTIR spectrum. At first, the CV curves were measured in 0.1 M PBS (pH=7) with DA concentration of 50 μM, 100 μM, 150 μM, 200 μM, 250 μM and 300 μM at the scan rate of 100 mV/s. From the CV curves shown in Fig. 4a, the oxidation peaks showed up at a potential of 0.25 V due to DA oxidation and the peak current increased with the increasing of dopamine concentration. In order to simulate the DA fouling condition, this electrode was immersed in 1 mM DA solution for 5 min after the first round of CV test. Then, another series of CV curves were carried out at the same condition as previous one. From Fig. 4b, the current density of fouled electrode decreased obviously compared to that of the pristine one, because DA was easy to stick on the electrode surface and form into insulation film which reduced effective reaction area of DA oxidation [54]. To keep the measurement results accurate, dopamine fouling should be removed. To remove DA contamination from the electrode surface, a 5-min ultrasonic clean was conducted in deionized water to the fouled electrode. After ultrasonic (Fig. 4c), CV curves showed almost the same shape as the origin one, which revealed good recovery. In Fig. 4d, CV curves of the origin electrode, DA fouled electrode and electrode after ultrasonic cleaning were tested in 300 μM DA solution. Compared with the original sensor, the current peak of DA fouled one decreased by 49.2%, while the sensor after 5-min ultrasonic cleaning exhibit almost the same level (only 0.4% in current change) as before. The linear relationship between oxidation peak and DA concentration was summarized in Fig. 4e, in which the linear regression equation of the origin electrode, DA fouled electrode and ultrasonic cleaned electrode were expressed as ipa (μA/cm^2) = 235.38802 + 0.58031C (μM) (R^2 = 0.996) (equ.1), ipa (μA/cm^2) = 112.15449 + 0.30591C (μM) (R^2 = 0.993) (equ.2), ipa (μA/cm^2) = 236.51618 + 0.57075C (μM) (R^2 = 0.996) (equ.3), respectively. The slope and intercept of equ.2 and equ.1 were significantly different, while the slope and intercept of equ.3
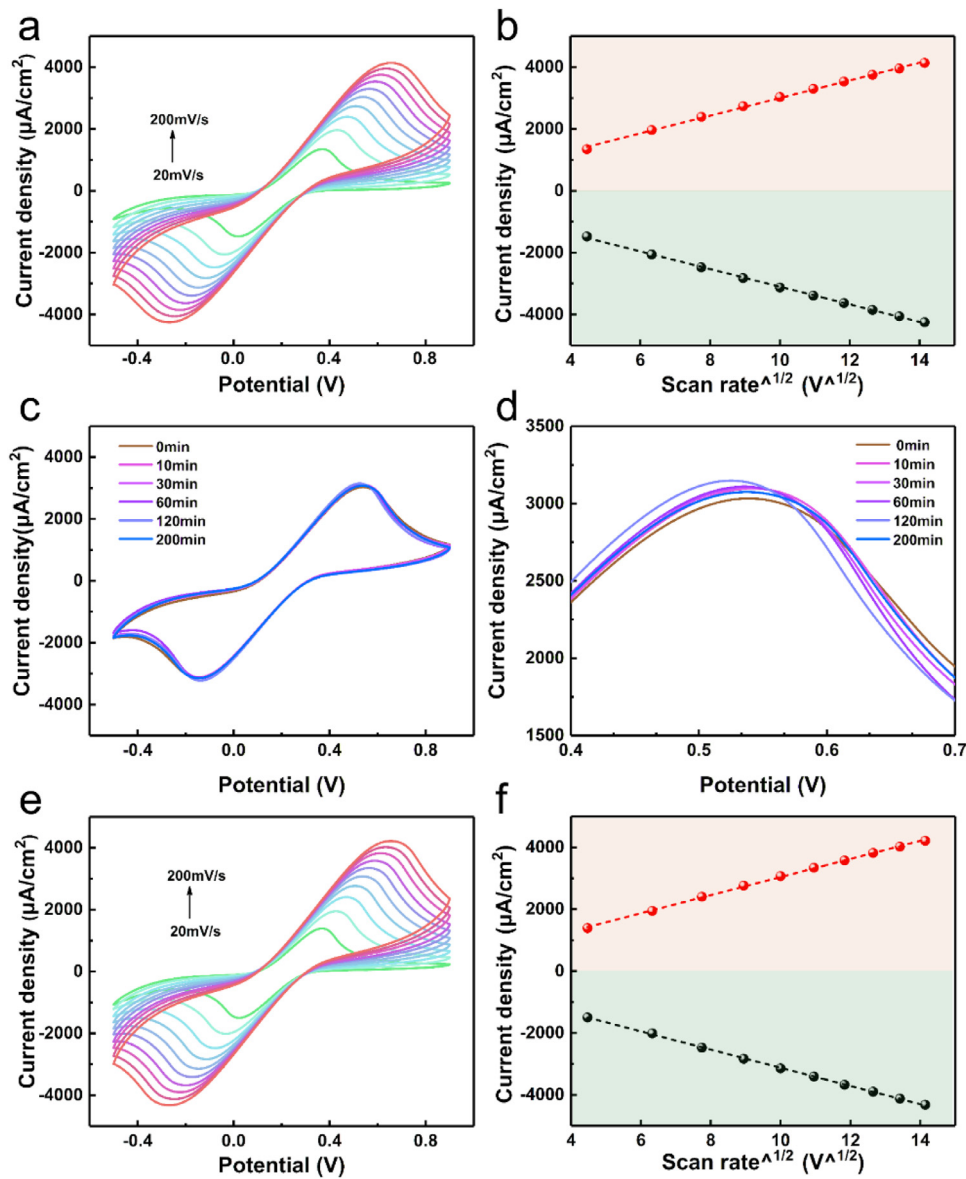
Fig. 3. CV curves of the as prepared electrode in 1 M HCl solution containing 10 mM K$_3$[Fe(CN)$_6$] with the scan rate from 20 mv/s to 200 mv/s (a);the relationship between current peak and square root of scan rate conducted on the pristine electrode (b); CV curves of different ultrasonic time (c) and magnified view of oxidation peak current position (d); CV curves (e) and linear relationship between current density peak and square root of scan rate after 200 min ultrasonic cleaning with the scan rate from 20 mv/s to 200 mv/s (f).

and equ.1 showed no significant difference, which confirmed the outstanding recovery of detection performance again. To identify the DA contamination and cleaning effect of the electrode surface, FTIR of the origin, fouled and ultrasonic cleaned electrode material surface were measured (shown in Fig. 4f). According to the FTIR spectroscopy, the fingerprints characteristic peaks of dopamine displayed on the DA fouled electrode surface compared to the origin one, which appeared at 1286 cm^{-1} and 1500 cm^{-1}, indicating the DA fouling was stick on electrode surface after 5-min immerse in 1 mM DA solution [38]. However, after 5-min ultrasonic bath in DI water, DA characteristic peaks disappeared, manifesting that dopamine contamination has been fully eliminated, which was the main reason for the recovery of DA detection ability. The rebirth of DA detection property illustrated that this porous carbon could be an ideal material for detection of fouling reagent DA and ultrasonic cleaning provided an effective way to clean up dopamine contamination and make the electrode regenerated.

2.3. Performance of DA detection

The performance of porous carbon electrode for DA detection was explored by differential pulse voltammetry (DPV) method in 0.1 M PBS (pH=7). Fig. 5a showed the DPV curves of different DA concentration, in which the anodic peak current showed up at 0.19 V and increased with DA level, ranging from 100 nM to 400 μM. Fig. 5b illustrated the relationship between peak current and DA concentration, in which the peak current was linear to DA concentration from 800 nM to 400 μM, with the linear regression equation represented as i$_{pa}$ (μA/cm^2) = $-0.24165 + 0.92134$C (μM) (R^2 = 0.998). Therefore, the linear range of DA sensing is 800 nM to 400 μM and the sensitivity is 0.92 μA/(cm$^2 \cdot \mu$M) revealed from the equation slope. Another important parameter was detection limit, which could be demonstrated as 100 nM. Table 1 showed the performance comparison of DA electrochemical sensing between our sensor and other active DA sensors.
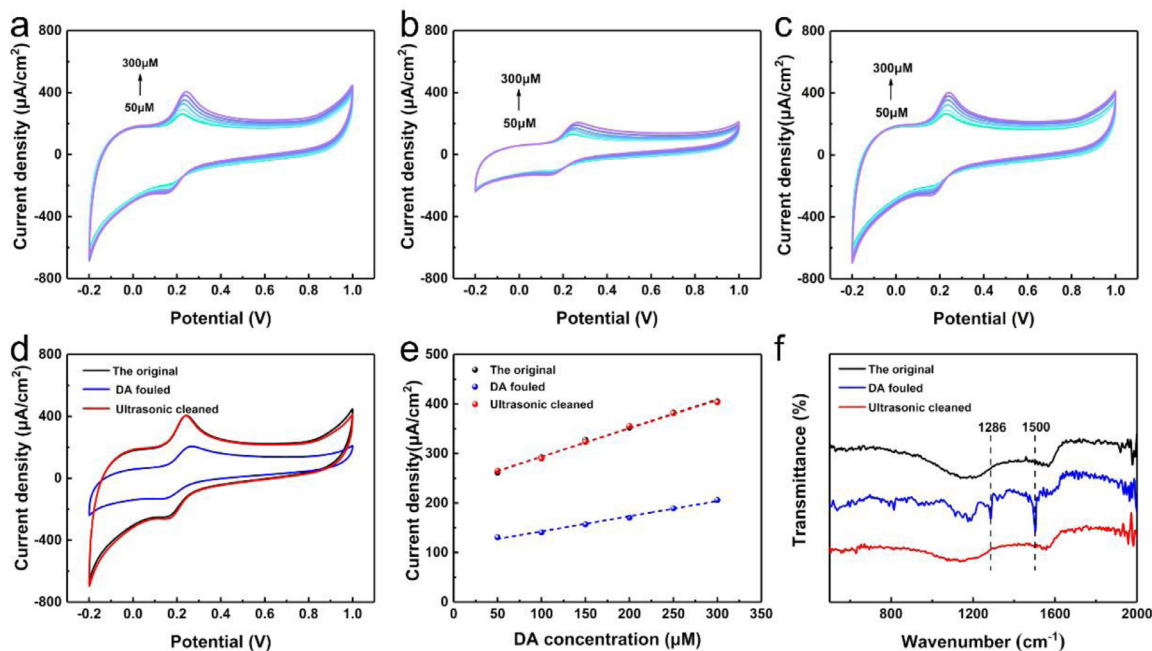
Fig. 4. CV curves in 0.1 M PBS (pH=7) containing DA from 50 μM to 300 μM of the origin electrode (a), electrode after dopamine fouling (b) and electrode after 5 min ultrasonic bath (c). Comparison of CV curves (d), relationship between peak current and DA concentration (e) of the origin electrode, fouled electrode and ultrasonic cleaned electrode. (f) FTIR transmission spectrum of the origin electrode, fouled electrode and ultrasonic cleaned electrode.
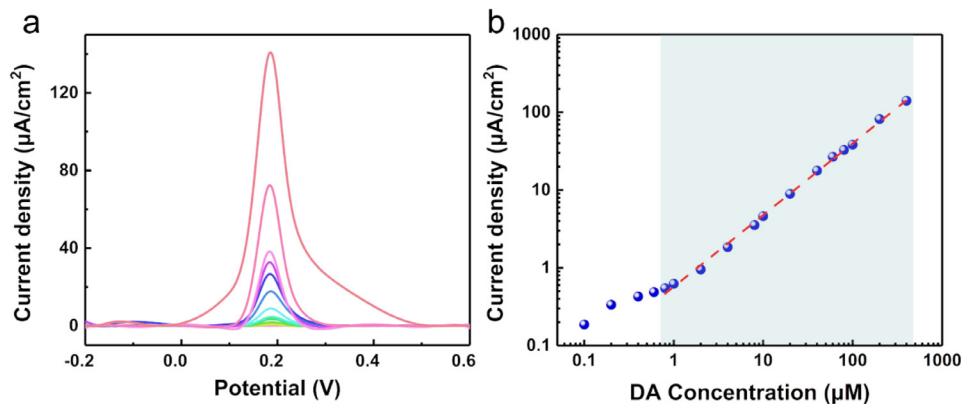

Fig. 5. (a) DPV curves of different DA concentration from 100 nM to 400 μM in 0.1 M PBS (pH=7). (b) the linear relation of current peak and DA concentration.

Table 1
Performance comparison of DA electrochemical sensing between this sensor and other active DA sensors.

Electrode	Methods	LOD(μM)	Linear range(μM)	ref
GO/GCE	DPV	0.27	1.0–15	[32]
SWCNT/PET	DPV	0.51	1.5–30	[23]
Au/RGO/GCE	DPV	1.4	6.8–41	[55]
graphene nano-sheets (GNSs)	DPV	0.6	4–52	[56]
RGO/PAMAM/MWCNT/AuNP/GCE	DPV	3.3	10–320	[57]
Graphene nanobelts/GCE	amperometry	0.58	2.0–202	[58]
3D N, P-doped carbon	DPV	0.6	2–200	[59]
N-rGO/GCE	DPV	0.41	0.5–150	[60]
N-doped graphene/GCE	DPV	0.25	0.5–170	[61]
3D PC	DPV	0.1	0.8–400	This work

Compared with other carbon-based DA sensors, such as graphene/GCE, graphene oxide/GCE and CNT electrode, this porous carbon sensor showed lower detection limit and wider linear range. Thanks to the large surface area and good mass transfer ability, the porous carbon electrode showed good sensitivity to DA, which was qualified for constructing DA detection platform.

To investigate the DA selectivity of porous carbon electrode, chronoamperometry was conducted in 0.1 M phosphate buffer solution (pH=7.0) at a given potential of 0.225 V. Possible interference substances such as ascorbic acid (AA), uric acid (UA), glucose (Glu), KCl, MgSO$_4$ and NaCl were added to simulate the interferences. The concentrations of AA, UA and Glu-were set as 1 mM,
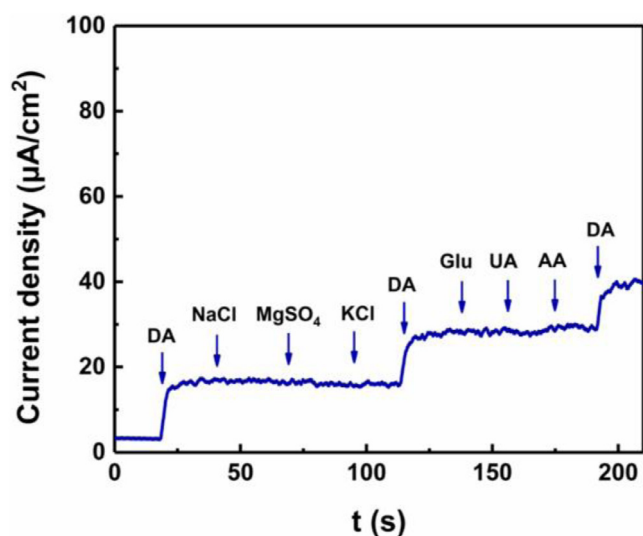
Fig. 6. Chronoamperometry responses of porous carbon electrode in 0.1 M PBS at 0.225 V with addition of DA, NaCl, MgSO4, KCl, Glu, UA and AA.

Table 2
Reproducibility of porous carbon electrodes.

Electrode number	1	2	3	4	5	6
Current density ($\mu A/cm^2$)	22.02	21.62	22.28	22.23	23.19	22.72
Average current density ($\mu A/cm^2$)	22.34					
RSD	2.46%					

Table 3
Repeatability of porous carbon electrodes.

Sample number	1	2	3	4	5	6
Current density ($\mu A/cm^2$)	22.56	22.57	22.48	22.48	22.14	22.81
Average current density ($\mu A/cm^2$)	22.51					
RSD	0.97%					

evaluated by measuring the DPV current signals to 50 μM DA of six independent solutions as was shown in Fig.S9b and Table 3. The RSD was 0.97% for the electrode implying reliable sensor performances.

4. Conclusion

In summary, a 3D hierarchical porous carbon sheet was synthetized through dual-template strategy with PET fibric and tri-block polymer F127 as hard and soft template, respectively. A hierarchical porous structure with macropores and ordered mesopores as well as the high sp^2 content were characterized. Then an electrochemical sensor for DA was established by overall porous carbon sheet. Instead of using drop-casting method, this porous carbon sensor was constructed by overall 3D framework, exhibiting good ultrasonic stability even after 200-min ultrasonic cleaning. According to the ultrasonic simulation experiment, 5-min ultrasonic cleaning process could fully eliminate dopamine pollutants on sensor surface and enable good recovery of DA oxidation ability. Such a porous carbon sensor exhibited excellent performance in electrochemical sensing to DA with a wide linear range from 800 nM to 400 μM, low detection limit of 100 nM and good selectivity to routine interference substances. Therefore, the excellent sensing performance and the good recovery toward DA detection manifest that the porous carbon sensor is promising in electrochemical detection platform construction of DA.

Declaration of Competing Interest

We have no conflicts of interest to this work.

CRediT authorship contribution statement

Shuyuan Wang: Conceptualization, Methodology, Data curation, Software, Writing - original draft, Writing - review & editing. **Peng Guo:** Conceptualization, Writing - review & editing. **Guanshui Ma:** Methodology, Writing - review & editing. **Jing Wei:** Data curation, Software. **Zhenyu Wang:** Data curation. **Li Cui:** Data curation. **Lili Sun:** Conceptualization, Methodology, Supervision. **Aiying Wang:** Conceptualization, Methodology, Writing - review & editing, Supervision, Funding acquisition.

Supplementary materials

Supplementary material associated with this article can be found, in the online version, at doi:10.1016/j.electacta.2020.137016.

50 µM and 5 mM, respectively, which corresponded to the maximum physiological concentrations of AA and UA in the human brain and normal level of Glu-in human blood [62-67]. And the concentrations of K$^+$, Mg^{2+} and Na$^+$ were set according to the typical level in human serum [68,69]. As illustrated in Fig. 6, an obvious amperometric response showed up when 200 μM DA was added, while no significant amperometric signal appeared with the addition of 140 mM NaCl, 1 mM MgSO$_4$, 5 mM KCl, 5 mM Glu, 50 µM UA and 1 mM AA, even the concentrations of interfering molecular were several times higher than DA. And the current increased again when 200 μM DA was added once more, thus suggesting that the as prepared porous carbon electrode showed excellent selectivity towards DA electrochemical detection. DPV measurements were also performed for the main interferences AA, UA and Glu. As was shown in Fig.S8, the peak current signal for DA (0.2 mM) was much stronger than that of AA (1 mM) and UA (50 μM), even AA concentration was 5 times higher than that of DA. And almost no signal was found in Glu-solution, even the concentration of Glu (5 mM) was 25 times higher than that of DA. The current changes in DA and interferences hybrid solutions were calculated to be 2.8% decrease for AA, 4.9% decrease for UA and 0.9% increase for Glu, respectively, which were quite slight and within acceptable range.

2.4. Stability, reproducibility and repeatability

The stability of the porous carbon electrode was tested during a period of storing in 0.1 M PBS solution (pH= 7.0) at room temperature (25 °C) for 12 days by measuring the DPV current of 50 μM DA. At the 12th day, it still retained 96.8% of its initial current signal (Fig.S7), which implied good stability of the porous carbon electrode. Six porous carbon electrodes were fabricated and their DPV current responses to 50 μM DA were investigated, in which the relative standard deviation (RSD) was 2.46% (Fig.S9a, Table 2), demonstrating the excellent reproducibility. The repeatability was

References

[1] R.M. Wightman, L.J. May, A.C. Michael, Detection of dopamine dynamics in the brain, Anal. Chem. 60 (1988) 769A–779A, https://doi.org/10.1021/ac00164a001.

[2] J.M. Savitt, V.L. Dawson, T.M. Dawson, Diagnosis and treatment of Parkinson disease: molecules to medicine, J. Clin. Invest. 116 (2006) 1744–1754, https://doi.org/10.1172/JCI29178.

[3] A. Carlsson, M. Lindqvist, T. Magnusson, 3,4Dihydroxyphenylalanine and 5Hydroxytryptophan as Reserpine Antagonists, Nature 180 (1957) 1200-1200, https://doi.org/10.1038/1801200a0 .

[4] E.E. Ferapontova, Electrochemical Analysis of Dopamine: perspectives of Specific In Vivo Detection, Electrochim. Acta 245 (2017) 664–671, https://doi.org/10.1016/j.electacta.2017.05.183.

[5] M.P. dos Santos, A. Rahim, N. Fattori, L.T. Kubota, Y. Gushikem, Novel amperometric sensor based on mesoporous silica chemically modified with ensal copper complexes for selective and sensitive dopamine determination, Sens. Actuator B-Chem. 171 (2012) 712–718, https://doi.org/10.1016/j.snb.2012.05.061.

[6] A. Naccarato, E. Gionfriddo, G. Sindona, A. Tagarelli, Development of a simple and rapid solid phase microextraction-gas chromatography-triple quadrupole mass spectrometry method for the analysis of dopamine, serotonin and norepinephrine in human urine, Anal. Chim. Acta 810 (2014) 17–24, https://doi.org/10.1016/j.aca.2013.11.058.

[7] H. Duan, L. Li, X. Wang, Y. Wang, J. Li, C. Luo, A sensitive and selective chemiluminescence sensor for the determination of dopamine based on silanized magnetic graphene oxide-molecularly imprinted polymer, Spectrochimica Acta Part a-Molecular and Biomolecular Spectroscopy 139 (2015) 374–379, https://doi.org/10.1016/j.saa.2014.12.051.

[8] J.-M. Liu, X.-X. Wang, M.-L. Cui, L.-P. Lin, S.-L. Jiang, L. Jiao, L.-H. Zhang, A promising non-aggregation colorimetric sensor of AuNRs-Ag+ for determination of dopamine, Sens. Actuator B-Chem. 176 (2013) 97–102, https://doi.org/10.1016/j.snb.2012.08.083.

[9] M.G. Garcia, G.M.E. Armendariz, L.A. Godinez, J. Torres, S. Sepulveda-Guzman, E. Bustos, Detection of dopamine in non-treated urine samples using glassy carbon electrodes modified with PAMAM dendrimer-Pt composites, Electrochim. Acta 56 (2011) 7712–7717, https://doi.org/10.1016/j.electacta.2011.06.035.

[10] B. Dinesh, R. Saraswathi, A.S. Kumar, Water based homogenous carbon ink modified electrode as an efficient sensor system for simultaneous detection of ascorbic acid, dopamine and uric acid, Electrochim. Acta 233 (2017) 92–104, https://doi.org/10.1016/j.electacta.2017.02.139.

[11] M. Maminski, M. Olejniczak, M. Chudy, A. Dybko, Z. Brzozka, Spectrophotometric determination of dopamine in microliter scale using microfluidic system based on polymeric technology, Anal. Chim. Acta 540 (2005) 153–157, https://doi.org/10.1016/j.aca.2004.09.011.

[12] Y.N. Park, X. Zhang, S.S. Rubakhin, J.V. Sweedler, Independent optimization of capillary electrophoresis separation and native fluorescence detection conditions for indolamine and catecholamine measurements, Anal. Chem. 71 (1999) 4997–5002, https://doi.org/10.1021/ac990659r.

[13] F.D.P. Ferreira, L.I.B. Silva, A.C. Freitas, T.A.P. Rocha-Santos, A.C. Duarte, High performance liquid chromatography coupled to an optical fiber detector coated with laccase for screening catecholamines in plasma and urine, Journal of Chromatography A 1216 (2009) 7049–7054, https://doi.org/10.1016/j.chroma.2009.08.067.

[14] J. Feng, Q. Li, J. Cai, T. Yang, J. Chen, X. Hou, Electrochemical detection mechanism of dopamine and uric acid on titanium nitride-reduced graphene oxide composite with and without ascorbic acid, Sens. Actuator B-Chem. 298 (2019), https://doi.org/10.1016/j.snb.2019.126872.

[15] X. Mei, Q. Wei, H. Long, Z. Yu, Z. Deng, L. Meng, J. Wang, J. Luo, C.-.T. Lin, L. Ma, K. Zheng, N. Hu, Long-term stability of Au nanoparticle-anchored porous boron-doped diamond hybrid electrode for enhanced dopamine detection, Electrochim. Acta 271 (2018) 84–91, https://doi.org/10.1016/j.electacta.2018.03.133.

[16] Carbon Nanomaterials for Neuroanalytical Chemistry, Nanocarbons for Electroanalysis, pp. 55–83.

[17] Y. Hei, X. Li, X. Zhou, J. Liu, M. Hassan, S. Zhang, Y. Yang, X. Bo, H.-.L. Wang, M. Zhou, Cost-effective synthesis of three-dimensional nitrogen-doped nanostructured carbons with hierarchical architectures from the biomass of seatangle for the amperometric determination of ascorbic acid, Anal. Chim. Acta 1029 (2018) 15–23, https://doi.org/10.1016/j.aca.2018.05.041.

[18] T. Laurila, S. Sainio, M.A. Caro, Hybrid carbon based nanomaterials for electrochemical detection of biomolecules, Prog Mater Sci 88 (2017) 499–594, https://doi.org/10.1016/j.pmatsci.2017.04.012.

[19] J. Gao, Q. Yuan, C. Ye, P. Guo, S. Du, G. Lai, A. Yu, N. Jiang, L. Fu, C.-.T. Lin, K.W.A. Chee, Label-Free Electrochemical Detection of Vanillin through Low-Defect Graphene Electrodes Modified with Au Nanoparticles, Materials (Basel) 11 (2018), https://doi.org/10.3390/ma11040489.

[20] J. Gao, H. Zhang, C. Ye, Q. Yuan, K.W.A. Chee, W. Su, A. Yu, J. Yu, C.-.T. Lin, D. Dai, L. Fu, Electrochemical Enantiomer Recognition Based on sp-to-sp Converted Regenerative Graphene/Diamond Electrode, Nanomaterials (Basel) 8 (2018), https://doi.org/10.3390/nano8121050.

[21] S. Pruneanu, A.R. Biris, F. Pogacean, C. Socaci, M. Coros, M.C. Rosu, F. Watanabe, A.S. Biris, The influence of uric and ascorbic acid on the electrochemical detection of dopamine using graphene-modified electrodes, Electrochim. Acta 154 (2015) 197–204, https://doi.org/10.1016/j.electacta.2014.12.046.

[22] Y. Haldorai, A.T.E. Vilian, M. Rethinasabapathy, Y.S. Huh, Y.-.K. Han, Electrochemical determination of dopamine using a glassy carbon electrode modified with TiN-reduced graphene oxide nanocomposite, Sens. Actuator B-Chem. 247 (2017) 61–69, https://doi.org/10.1016/j.snb.2017.02.181.

[23] J.-.W. Oh, J. Heo, T.H. Kim, An electrochemically modulated single-walled carbon nanotube network for the development of a transparent flexible sensor for dopamine, Sens. Actuator B-Chem. 267 (2018) 438–447, https://doi.org/10.1016/j.snb.2018.04.048.

[24] X. Zhang, L.-.X. Ma, Y.-.C. Zhang, Electrodeposition of platinum nanosheets on C-60 decorated glassy carbon electrode as a stable electrochemical biosensor for simultaneous detection of ascorbic acid, dopamine and uric acid, Electrochim. Acta 177 (2015) 118–127, https://doi.org/10.1016/j.electacta.2015.01.202.

[25] X. Zhang, J. Zheng, Hollow carbon sphere supported Ag nanoparticles for promoting electrocatalytic performance of dopamine sensing, Sens. Actuator B-Chem. 290 (2019) 648–655, https://doi.org/10.1016/j.snb.2019.04.040.

[26] L. Zhao, Z. Cai, Q. Yao, T. Zhao, H. Lin, Y. Xiao, X. Chen, Electropolymerization fabrication of three-dimensional, P-co-doped carbon network as a flexible electrochemical dopamine sensor, Sens. Actuator B-Chem. 253 (2017) 1113–1119, https://doi.org/10.1016/j.snb.2017.06.111.

[27] X. Zhu, B. Liu, L. Wu, S. Chen, J. Yang, S. Liang, K. Xiao, J. Hu, H. Hou, Synthesis of 3D hierarchically porous carbon@Bi-BiOCl nanocomposites via in situ generated NaCl crystals as templates for highly sensitive detection of Pb2+ and Cd2+, Electrochim. Acta 318 (2019) 460–470, https://doi.org/10.1016/j.electacta.2019.06.098.

[28] C.X. Xu, Y.S. Hei, J.J. Liu, M.M. Sun, T.Z. Sha, N. Wang, M. Hassan, X.J. Bo, M. Zhou, Synthesis of a three-dimensional interconnected carbon nanorod aerogel from wax gourd for amperometric sensing, Microchim. Acta 185 (2018) 12, https://doi.org/10.1007/s00604-018-3008-y.

[29] Q. Cao, P. Puthongkham, B.J. Venton, Review: new insights into optimizing chemical and 3D surface structures of carbon electrodes for neurotransmitter detection, Analytical Methods 11 (2019) 247–261, https://doi.org/10.1039/c8ay02472c.

[30] A. Brouzgou, E. Gorbova, Y. Wang, S. Jing, A. Seretis, Z. Liang, P. Tsiakaras, Nitrogen-doped 3D hierarchical ordered mesoporous carbon supported palladium electrocatalyst for the simultaneous detection of ascorbic acid, dopamine, and glucose, Ionics (Kiel) 25 (2019) 6061–6070, https://doi.org/10.1007/s11581-019-03116-z.

[31] L. Dong, L. Fan, Y. Ding, Hierarchical Porous Carbon Derived from Pyrolysis of Sodium Citrate for Sensitive Determination of Dopamine and Uric Acid, J Electrochem Soc 166 (2019) B1585–B1593, https://doi.org/10.1149/2.1341914jes.

[32] S. Liu, S. Gao, T. Fei, T. Zhang, Highly Sensitive and Selective Dopamine Detection Utilizing Nitrogen-Doped Mesoporous Carbon Prepared by a Molten Glucose-Assisted Hard-Template Approach, Chempluschem 84 (2019) 845–852, https://doi.org/10.1002/cplu.201900291.

[33] E. Peltola, S. Sainio, K.B. Holt, T. Palomaki, J. Koskinen, T. Laurila, Electrochemical Fouling of Dopamine and Recovery of Carbon Electrodes, Anal. Chem. 90 (2018) 1408–1416, https://doi.org/10.1021/acs.analchem.7b04793.

[34] R. Trouillon, Y. Einaga, M.A.M. Gijs, Cathodic pretreatment improves the resistance of boron-doped diamond electrodes to dopamine fouling, Electrochem commun 47 (2014) 92–95, https://doi.org/10.1016/j.elecom.2014.07.028.

[35] S. Chandra, A.D. Miller, A. Bendavid, P.J. Martin, D.K.Y. Wong, Minimizing Fouling at Hydrogenated Conical-Tip Carbon Electrodes during Dopamine Detection in Vivo, Anal. Chem. 86 (2014) 2443–2450, https://doi.org/10.1021/ac403283t.

[36] T. Palomaki, S. Chumillas, S. Sainio, V. Protopopova, M. Kauppila, J. Koskinen, V. Climent, J.M. Feliu, T. Laurila, Electrochemical reactions of catechol, methylcatechol and dopamine at tetrahedral amorphous carbon (ta-C) thin film electrodes, Diam Relat Mater 59 (2015) 30–39, https://doi.org/10.1016/j.diamond.2015.09.003.

[37] S. Chumillas, T. Palomaki, M. Zhang, T. Laurila, V. Climent, J.M. Feliu, Analysis of catechol, 4-methylcatechol and dopamine electrochemical reactions on different substrate materials and pH conditions, Electrochim. Acta 292 (2018) 309–321, https://doi.org/10.1016/j.electacta.2018.08.113.

[38] Q. Yuan, Y. Liu, C. Ye, H. Sun, D. Dai, Q. Wei, G. Lai, T. Wu, A. Yu, L. Fu, K.W.A. Chee, C.-.T. Lin, Highly stable and regenerative graphene-diamond hybrid electrochemical biosensor for fouling target dopamine detection, Biosens. Bioelectron. 111 (2018) 117–123, https://doi.org/10.1016/j.bios.2018.04.006.

[39] L. Wang, H. Yang, L. Xu, C. Peng, Y. Song, A novel popamine-imprinted chitosan/CuCo2O4@carbon/three-dimensional macroporous carbon integrated electrode, J Alloys Compd 817 (2020), https://doi.org/10.1016/j.jallcom.2019.152771.

[40] V. Veeramani, R. Madhu, S.-.M. Chen, B.-.S. Lou, J. Palanisamy, V.S. Vasantha, Biomass-derived functional porous carbons as novel electrode material for the practical detection of biomolecules in human serum and snail hemolymph, Sci Rep 5 (2015), https://doi.org/10.1038/srep10141.

[41] V. Sudha, S.M.S. Kumar, R. Thangamuthu, Hierarchical porous carbon derived from waste amla for the simultaneous electrochemical sensing of multiple biomolecules, Colloids and Surfaces B-Biointerfaces 177 (2019) 529–540, https://doi.org/10.1016/j.colsurfb.2019.01.029.

[42] Q. Cheng, L. Ji, K. Wu, W. Zhang, Morphology-dependent Electrochemical Enhancements of Porous Carbon as Sensitive Determination Platform for Ascorbic Acid, Dopamine and Uric Acid, Sci Rep 6 (2016), https://doi.org/10.1038/srep22309.

[43] C. Xiang, Y. Zou, L.-.X. Sun, F. Xu, Direct electrochemistry and enhanced electrocatalysis of horseradish peroxidase based on flowerlike ZnO-gold nanoparticle-Nafion nanocomposite, Sens. Actuator B-Chem. 136 (2009) 158–162, https://doi.org/10.1016/j.snb.2008.10.058.

[44] Y. Jiao, S.W. Cho, S. Lee, S.H. Kim, S.-.Y. Jeon, K. Hur, S.M. Yoon, M.-.W. Moon, A. Wang, A Hierarchically Porous Carbon Fabric for Highly Sensitive Electrochemical Sensors, Adv Eng Mater 20 (2018), https://doi.org/10.1002/adem.201700608.

[45] A.-.H. Lu, B. Spliethoff, F. Schueth, Aqueous Synthesis of Ordered Mesoporous Carbon via Self-Assembly Catalyzed by Amino Acid, Chemistry of Materials 20 (2008) 5314–5319, https://doi.org/10.1021/cm800362g.

[46] Y. Chi, J. Tu, M. Wang, X. Li, Z. Zhao, One-pot synthesis of ordered mesoporous silver nanoparticle/carbon composites for catalytic reduction of 4-nitrophenol, J Colloid Interface Sci 423 (2014) 54–59, https://doi.org/10.1016/j.jcis.2014.02.029.

[47] H.-.Q. Li, R.-.L. Liu, D.-.Y. Zhao, Y.-.Y. Xia, Electrochemical properties of an ordered mesoporous carbon prepared by direct tri-constituent co-assembly, Carbon N Y 45 (2007) 2628–2635, https://doi.org/10.1016/j.carbon.2007.08.005.

[48] R. Madhu, V. Veeramani, S.-.M. Chen, Heteroatom-enriched and renewable banana-stem-derived porous carbon for the electrochemical determination of nitrite in various water samples, Sci Rep 4 (2014), https://doi.org/10.1038/srep04679.

[49] R. Madhu, K.V. Sankar, S.-.M. Chen, R.K. Selvan, Eco-friendly synthesis of activated carbon from dead mango leaves for the ultrahigh sensitive detection of toxic heavy metal ions and energy storage applications, RSC Adv 4 (2014) 1225–1233, https://doi.org/10.1039/c3ra45089a.

[50] E. Ramasamy, J. Chun, J. Lee, Soft-template synthesized ordered mesoporous carbon counter electrodes for dye-sensitized solar cells, Carbon N Y 48 (2010) 4563–4565, https://doi.org/10.1016/j.carbon.2010.07.030.

[51] E.P. Barrett, L.G. Joyner, P.P. Halenda, THE DETERMINATION OF PORE VOLUME AND AREA DISTRIBUTIONS IN POROUS SUBSTANCES .1. COMPUTATIONS FROM NITROGEN ISOTHERMS, J. Am. Chem. Soc. 73 (1951) 373–380, https://doi.org/10.1021/ja01145a126.

[52] A.J. Bard, L.R. Faulkner, Electrochemical Methods, Fundamentals & Applications, Wiley*, 1980.

[53] Y. Huang, Y. Zhang, D. Liu, M. Li, Y. Yu, W. Yang, H. Li, Facile synthesis of highly ordered mesoporous Fe3O4 with ultrasensitive detection of dopamine, Talanta 201 (2019) 511–518, https://doi.org/10.1016/j.talanta.2019.01.099.

[54] W. Harreither, R. Trouillon, P. Poulin, W. Neri, A.G. Ewing, G. Safina, Carbon Nanotube Fiber Microelectrodes Show a Higher Resistance to Dopamine Fouling, Anal. Chem. 85 (2013) 7447–7453, https://doi.org/10.1021/ac401399s.

[55] C. Wang, J. Du, H. Wang, C.E. Zou, F. Jiang, P. Yang, Y. Du, A facile electrochemical sensor based on reduced graphene oxide and Au nanoplates modified glassy carbon electrode for simultaneous detection of ascorbic acid, dopamine and uric acid, Sens. Actuator B-Chem. 204 (2014) 302–309, https://doi.org/10.1016/j.snb.2014.07.077.

[56] S.-.Q. Liu, W.-.H. Sun, F.-.T. Hu, Graphene nano sheet-fabricated electrochemical sensor for the determination of dopamine in the presence of ascorbic acid using cetyltrimethylammonium bromide as the discriminating agent, Sens. Actuator B-Chem. 173 (2012) 497–504, https://doi.org/10.1016/j.snb.2012.07.052.

[57] S. Wang, W. Zhang, X. Zhong, Y. Chai, R. Yuan, Simultaneous determination of dopamine, ascorbic acid and uric acid using a multi-walled carbon nanotube and reduced graphene oxide hybrid functionalized by PAMAM and Au nanoparticles, Analytical Methods 7 (2015) 1471–1477, https://doi.org/10.1039/c4ay02086c.

[58] P.K. Kannan, S.A. Moshkalev, C.S. Rout, Highly sensitive and selective electrochemical dopamine sensing properties of multilayer graphene nanobelts, Nanotechnology 27 (2016), https://doi.org/10.1088/0957-4484/27/7/075504.

[59] X. Feng, Y. Zhang, J. Zhou, Y. Li, S. Chen, L. Zhang, Y. Ma, L. Wang, X. Yan, Three-dimensional nitrogen-doped graphene as an ultrasensitive electrochemical sensor for the detection of dopamine, Nanoscale 7 (2015) 2427–2432, https://doi.org/10.1039/c4nr06623e.

[60] P. Wiench, Z. Gonzalez, R. Menendez, B. Grzyb, G. Gryglewicz, Beneficial impact of oxygen on the electrochemical performance of dopamine sensors based on N-doped reduced graphene oxides, Sens. Actuator B-Chem. 257 (2018) 143–153, https://doi.org/10.1016/j.snb.2017.10.106.

[61] Z.H. Sheng, X.Q. Zheng, J.Y. Xu, W.J. Bao, F.B. Wang, X.H. Xia, Electrochemical sensor based on nitrogen doped graphene: simultaneous determination of ascorbic acid, dopamine and uric acid, Biosens. Bioelectron. 34 (2012) 125–131, https://doi.org/10.1016/j.bios.2012.01.030.

[62] P. Lyrer, H. Landolt, A. Kabiersch, H. Langemann, H. Kaeser, LEVELS OF LOW-MOLECULAR-WEIGHT SCAVENGERS IN THE RAT-BRAIN DURING FOCAL ISCHEMIA, Brain Res. 567 (1991) 317–320, https://doi.org/10.1016/0006-8993(91)90811-9.

[63] M.E. Rice, Ascorbate regulation and its neuroprotective role in the brain, Trends Neurosci 23 (2000) 209–216, https://doi.org/10.1016/s0166-2236(99)01543-x.

[64] D.L. Robinson, A. Hermans, A.T. Seipel, R.M. Wightman, Monitoring rapid chemical communication in the brain, Chem. Rev. 108 (2008) 2554–2584, https://doi.org/10.1021/cr068081q.

[65] S. Sainio, T. Palomaki, S. Rhode, M. Kauppila, O. Pitkanen, T. Selkala, G. Toth, M. Moram, K. Kordas, J. Koskinen, T. Laurila, Carbon nanotube (CNT) forest grown on diamond-like carbon (DLC) thin films significantly improves electrochemical sensitivity and selectivity towards dopamine, Sens. Actuator B-Chem. 211 (2015) 177–186, https://doi.org/10.1016/j.snb.2015.01.059.

[66] T. Palomaki, E. Peltola, S. Sainio, N. Wester, O. Pitkanen, K. Kordas, J. Koskinen, T. Laurila, Unmodified and multi-walled carbon nanotube modified tetrahedral amorphous carbon (ta-C) films as in vivo sensor materials for sensitive and selective detection of dopamine (vol 118, pg 23, 2018), Biosens. Bioelectron. 123 (2019) 281–284, https://doi.org/10.1016/j.bios.2018.08.053.

[67] Z. Khosroshahi, F. Karimzadeh, M. Kharaziha, A. Allafchian, A non-enzymatic sensor based on three-dimensional graphene foam decorated with Cu-xCu(2)O nanoparticles for electrochemical detection of glucose and its application in human serum, Materials Science & Engineering C-Materials for Biological Applications 108 (2020), https://doi.org/10.1016/j.msec.2019.110216.

[68] M. Walser, ION ASSOCIATION .6. INTERACTIONS BETWEEN CALCIUM, MAGNESIUM, INORGANIC PHOSPHATE, CITRATE AND PROTEIN IN NORMAL HUMAN PLASMA, J. Clin. Invest. 40 (1961) 723–&, https://doi.org/10.1172/jci104306 .

[69] Q.J. Wan, P. Kuban, J. Tanyanyiwa, A. Rainelli, P.C. Hauser, Determination of major inorganic ions in blood serum and urine by capillary electrophoresis with contactless conductivity detection, Anal. Chim. Acta 525 (2004) 11–16, https://doi.org/10.1016/j.aca.2004.08.002.